8.12 LARGE-EDDY SIMULATIONS AND OBSERVATIONS OF WAVE-DRIVEN BOUNDARY LAYERS

Peter P. Sullivan[1]*, James B. Edson[2], James C. McWilliams[3], and Chin-Hoh Moeng[1]

[1]National Center for Atmospheric Research, Boulder, CO
[2]Applied Ocean Physics and Engineering, Woods Hole Oceanographic Institute, Woods Hole, MA
[3]Department of Atmospheric and Oceanic Sciences, UCLA, Los Angeles, CA

1. INTRODUCTION

Air-sea interaction occurs over a wide spectrum of scales ranging from millimeters (spray droplets and air bubbles) to hundreds of kilometers (synoptic scale storms) and even larger (global climate). The coupling among water waves and atmospheric turbulence is one of the important components of air-sea interaction. Wind generated waves influence the flux of momentum and scalars at the air-sea interface and represent a visible signature of coupling between the atmosphere and ocean. Also, the fundamental difference between atmospheric boundary layers over land and over water derives from the scale and mobility of the water surface.

An outstanding question in wind-wave interaction is the impact of swell on the atmospheric planetary boundary layer (PBL). Swell dominated wave fields occur after the passage of storm fronts and can propagate long distances without significant dissipation, *e.g.,* see estimates in Cohen and Belcher (1999). In the open ocean, the wave height variance is typically dominated by swell (*i.e.,* by old waves) and as a result it is difficult to measure and isolate the contributions of young (short) waves to the roughness and surface stress. The impact of swell on surface drag parameterizations is correspondingly unsettled. A recent study by Donelan et al. (1997) suggests that swell influences are strong and that wind-swell alignment is an important factor for the measured drag coefficients (*e.g.,* they report that the drag increases by a factor of 3 for swell opposing the wind). Thus, the surface stress depends on at least three factors, wind speed, wave age, and swell.

The coupling between light winds following fast running swell is of particular interest here. Harris (1966) first reported the formation of a wave-driven wind in a laboratory wave tank. Later, Holland et al. (1981) and other observational campaigns noted an increase in surface winds in the presence of swell. Since then a growing body of experimental evidence has documented unique marine surface layer dynamics in the presence of swell; development of low-level jets (Holland et al. 1981; Miller 1999), positive upward momentum flux (Grachev and Fairall 2001; Smedman et al. 1994, 1999), negative mean profile gradients (Rutgersson et al., 2001), reduced turbulence levels (Drennan et al., 1999), and mis-alignment between surface stresses and mean winds (Grachev et al., 2003). These features appear to be signatures of a wave-driven surface layer and invalidate the use of Monin-Obukhov similarity theory most often used to predict air-sea fluxes (Rutgersson et al., 2001). The overall impact of swell is counter to the commonly accepted premise that the depth of the wave boundary layer (WBL), *i.e.,* the region directly impacted by waves, is quite shallow $z < 3$m (Makin and Mastenbroek, 1996).

The goals of the present work are to develop and use turbulence resolving simulations to improve our understanding of the interactions between atmospheric turbulence and surface waves, and to aid in the interpretation of observations from the Coupled Boundary Layers Air-Sea Transfer (CBLAST) field campaign, see Edson et al. (2004).

2. NUMERICAL MODEL AND PROBLEM DESIGN

To model the impact of surface waves on the atmospheric PBL, we have recently developed a new large-eddy simulation (LES) code with the capability of resolving moving sinusoidal modes imposed at its lower boundary. As the working flow model for this code we assume unsteady, 3D, incompressible Boussinesq equations with large scale pressure gradients provided by geostrophic winds. The LES equation set includes spatially filtered momentum $\rho\mathbf{u}$, potential temperature θ, and subgrid-scale (SGS) turbulent kinetic energy e equations (Moeng 1984; Sullivan et al. 1994). These equations are transformed from (x,y,z)-Cartesian coordinates into general surface fitted (computational) coordinates (ξ,η,ζ). Although arbitrary curvilinear grids are permitted, we restrict the grid to a conformal mesh which simplifies the solution of the pressure Poisson equation and

*corresponding author address: Peter P. Sullivan, National Center for Atmospheric Research, P. O. Box 3000, Boulder, CO 80307-3000; *email*: pps@ncar.ucar.edu

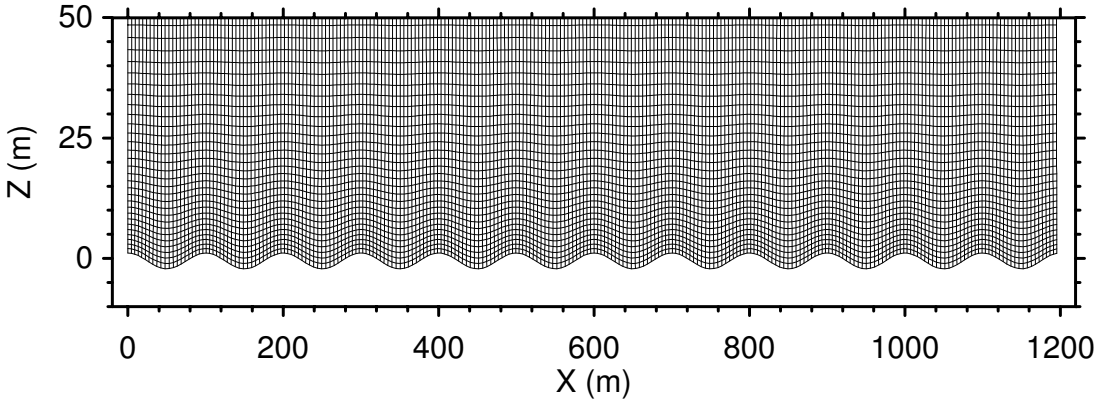

Figure 1: An $x-z$ slice of the conformal computational mesh in the lowest 50 meters used in the simulation of flow over water waves.

also allows for accurate treatment of the surface boundary conditions. For cases with moving lower boundaries, the surface fitted coordinate system propagates in the $x-$direction at the phase speed c of the imposed wave[1]. This strategy freezes the motion of the grid and allows us to easily include the orbital velocities of the water.

The base numerical algorithm in the present code borrows heavily from our direct numerical simulation (DNS) code for flow over stratified waves (Sullivan and McWilliams, 2002; Sullivan et al., 2000). A co-located (cell centered) arrangement of Cartesian solution variables $(\mathbf{u},\theta,p,e)$ is used along with contravariant flux velocities $\mathbf{U}$ oriented perpendicular to cell faces. The latter mimic the arrangement of variables on a staggered grid. Advantages of the co-located grid structure are: (1) all advective terms can be compactly discretized using a skew symmetric form, *e.g.,* momentum advection is $(\partial(U_j u_i)/\partial\xi_j + U_j\partial u_i/\partial\xi_j)/2$; and, (2) the location and orientation of $\mathbf{U}$, maintains tight velocity-pressure coupling as the continuity equation $\partial U_i/\partial\xi_i$ is used to construct the discrete pressure Poisson equation. A key difference between the LES and DNS is the formulation of the surface boundary condition. In the LES, a high-Reynolds number surface drag law based on a "z_o"-boundary condition is applied at the lower boundary, essentially a law-of-the-wall expression is applied instantaneously at every surface grid point using the surface parallel winds. Similar to the DNS code, the spatial discretizaion is pseudospectral in the surface following (ξ,η) coordinates and second-order finite difference in the vertical coordinate ζ. A third-order Runge-Kutta time stepping scheme operating with a fixed CFL number is employed (Sullivan et al., 1996). The entire code is parallelized using the Message Passing Interface (MPI) with domain decomposition in ζ. A custom built MPI matrix-transpose is used for the iterative solution of the pressure Poisson equation.

Conformal meshes are constructed using elliptic grid generation techniques, (*e.g.,* Thomson et al. 1985) with variable vertical spacing used to focus grid resolution near the surface (see Figure 1); algebraic stretching is employed with the stretching factor between two adjacent vertical cells $K = \Delta_{k+1}/\Delta_k = 1.036$. For the suite of LES experiments presented, the computational domain $(1200,1200,800)$m is discretized using $(250,250,96)$ gridpoints so that the horizontal resolution $(\Delta x,\Delta y) = (4.8,4.8)$m. As a result, the waveforms imposed at the lower boundary are well resolved, approximately 25 gridpoints per wave (see problem specification below). In the vertical direction, $\Delta\zeta = 1$m at the first gridpoint off the surface, and approximately 75 grid levels are located between the surface and the PBL inversion. Typically, at least 50,000 integration time steps are required to reach a statistically stationary state with the phase speed c limiting the allowable time step, $\Delta t \approx 0.23$s.

The LES code is used to simulate PBLs with a flat surface, and stationary and moving waves all with small surface roughness $z_o = 0.0002$m. This small value of z_o accounts for the drag of unresolved small scale waves riding on the larger scale resolved swell. The imposed surface wave is two-dimensional (*i.e.,* has $x-z$ variations) with wavelength $\lambda = 100$m and low waveslope $a2\pi/\lambda = 0.1$. Based on the linear dispersion relationship $c^2 = g\lambda/2\pi$, the moving wave has phase speed $c = 12.5\text{ms}^{-1}$ and propagates in the $x-$direction. The geostrophic wind $(U_g,V_g) = (5,0)\text{ms}^{-1}$ with Coriolis parameter $f = 10^{-4}\text{s}^{-1}$. Two values of surface heat flux are considered $Q_* = (0,0.01)\text{K-ms}^{-1}$. The initial depth of the PBL is $z_i = 400$m and the temperature sounding is $\partial\theta/\partial z = 0$ for $0 < z < z_i$ with a strong stable inversion $\partial\theta/\partial z = 0.01\text{Km}^{-1}$ above z_i. For this choice of

[1]This is common practice with second-order closure models for turbulent flow over waves *e.g.,* see Belcher and Hunt (1998).

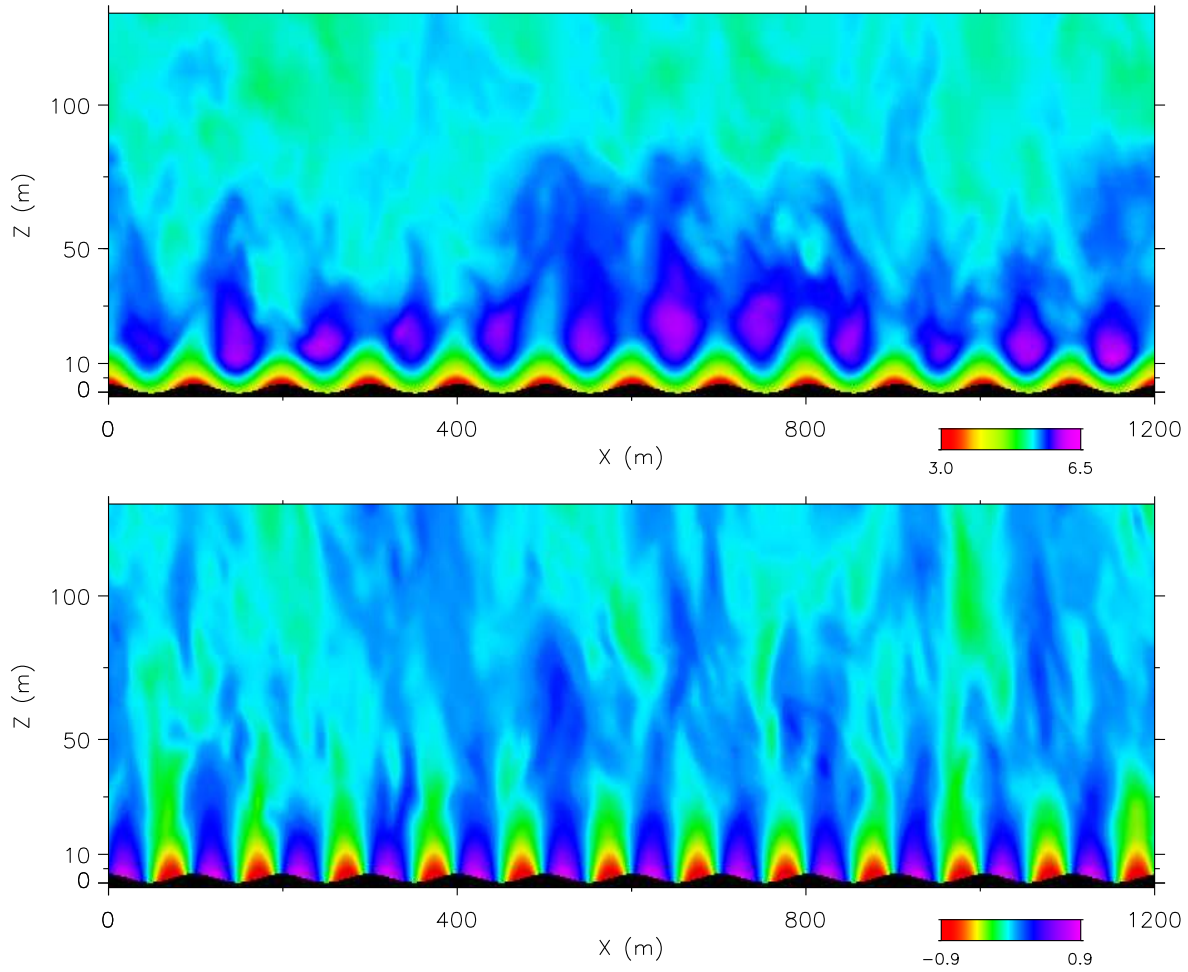

Figure 2: Snapshot of the instantaneous velocities over swell in neutrally stratified winds of 5ms^{-1} from LES. The wave age $c/U_{10} > 2.2$, where U_{10} is the wind at $z = 10$m and c is the wave phase speed. Upper panel u and lower panel w. Note the strong positive correlation between u and w on the downwind side of each wave crest which leads to a positive upward momentum flux uw above $z \approx 10$m. The color bar, located in the lower right portion of each figure, shows the variation in units of ms^{-1} The direction of wave propagation is to the right.

geostrophic winds and waves, the PBL is dominated by swell as the wave age $c/U_g > 2$ (*e.g.,* Drennan et al. 1999; Rutgersson et al. 2001). Thus our simulations are an idealization of the outdoor situation of light winds following strong swell. It is expected that turbulent flow overlying cross or counter swell will generate different flow dynamics.

3. RESULTS

Snapshots of the LES solutions provides striking visual evidence of the impact of swell on the PBL surface layer dynamics. Figure 2 shows that with fast running waves (wave age $c/U_{10} = 2.2$) a coherent pattern of accelerated winds greater than U_g occurs in the region above each wave trough, $5 < z < 25$m. At the same time, the u-winds slow over the wave crests. The vertical velocity is biased towards negative (positive) values upstream (downstream) of the wave crest, respectively. This phase relationship between (u,w) induces positive (upward) vertical momentum flux and leads to the development of a low-level jet. A strong pressure signal (not shown) extends to more than 50m above the surface in the swell dominated cases. Organized negative (positive) pressure signals occur over the wave crests (troughs) with a small asymmetry at the surface. The form stress, obtained by integration of the surface pressure, is positive, *i.e.,* the waves are accelerating the winds. Flow visualization of other LES solutions shows that the observed features are robust, they persist in the presence

of convection and with reductions in z_o. The (u,w) flow patterns found here are in sharp contrast to flow over a stationary hill (Belcher and Hunt, 1998) and suggest that the underlying waves can significantly modify the overlying turbulent flow over the bulk of what is traditionally referred to as the PBL surface layer, approximately $0 < z < 0.1 z_i$.

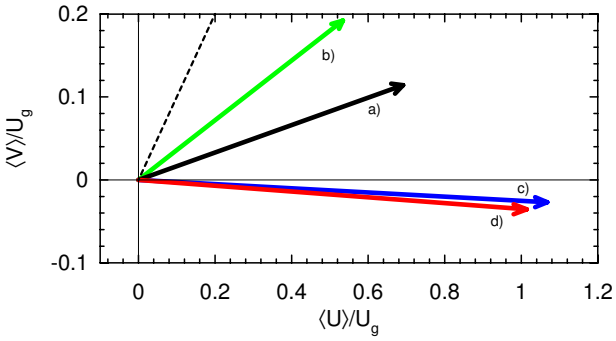

Figure 3: Wind vectors at $z = 10$m normalized by the geostrophic wind U_g for neutrally stratified flow over: a) flat surface; b) stationary wave; and, c) swell. Case d) is flow over swell with slight convection. The dashed line denotes an angle of 45 degrees between $\langle u \rangle$ and $\langle v \rangle$.

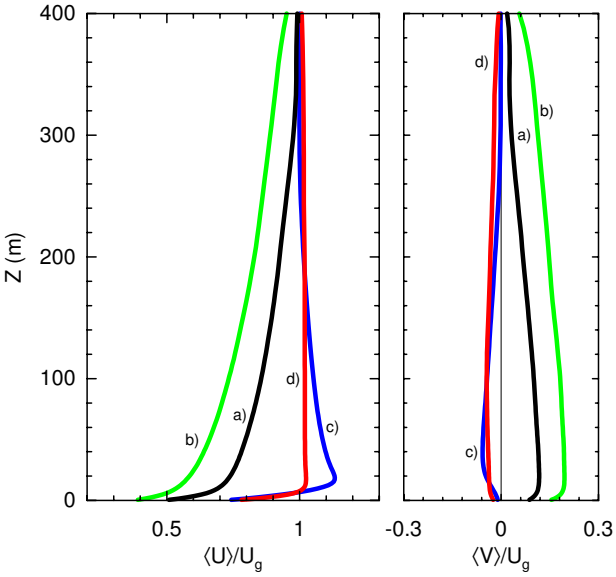

Figure 4: Vertical profiles of the mean wind for flow over waves. Temporal and spatial averaging is used to compute statistics with (spatial) horizontal averages carried out along $\zeta =$ constant surfaces. The labeling is identical to that used in Figure 3.

Further evidence for the impact of swell is presented in Figure 3, where the wind direction at $z = 10$m is displayed for four combinations of imposed surface waves (the magnitude and direction of the geostrophic wind, $\mathbf{U}_g = (U_g, 0)$, is held constant in each simulation). Over a flat surface with parameterized surface roughness the winds at $z = 10$m turn to the left as expected. The degree of turning increases in the presence of a stationary wave indicative of the increased surface layer stress due to the form drag of the underlying hills. However, an opposite trend is observed in the presence of swell; the winds turn slightly to the right in the surface layer ($\langle v \rangle < 0$) so that they are nearly aligned with the direction of swell propagation. The magnitude of the u-component also noticeably increases. The vertical profiles of the mean winds (see Figure 4) show that the impact of swell is not confined to the surface layer but can extend to considerable heights above the surface. With swell, the u-wind profile exhibits a low-level jet $\langle u \rangle / U_g > 1.1$ around $z = 20$m and then smoothly transitions to the geostrophic wind as $z \to 200$m. Hence, the mean shear above the jet is weak and slightly negative. In the presence of slight convection, the low-level jet nearly disappears, $\langle u \rangle \approx U_g$, and $\partial \langle u \rangle / \partial z \approx 0$ over the bulk of the PBL, $10\text{m} < z < 400\text{m}$. The flat surface and stationary hill cases both exhibit positive shear over the entire PBL. The weak mean shear in the swell driven (neutrally stratified) PBL generates only small amounts of turbulent kinetic energy in the region above the jet. As a result, the TKE nearly collapses in the upper PBL as a by-product of the swell induced changes in the marine surface layer.

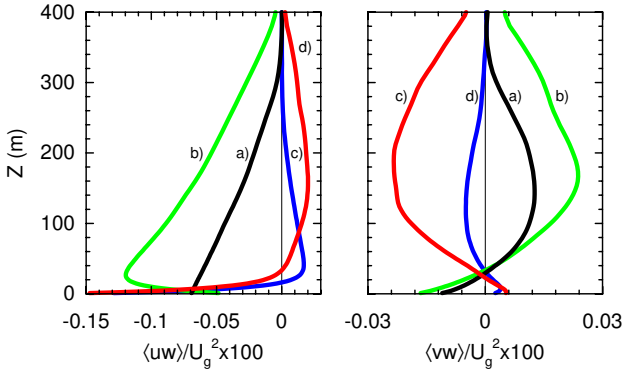

Figure 5: Total (resolved plus SGS) vertical momentum flux profiles. Note that the momentum fluxes are based on the W-velocity component normal to the $\zeta =$ constant surfaces. The labeling is identical to that shown in Figure 3.

Profiles of the total vertical momentum flux shown in Figure 5 illustrate the important consequences swell has for the momentum balance in the atmospheric PBL. In the presence of swell, the uW-component of the flux is negative very near the surface, rapidly approaches zero with increasing z, and eventually changes sign near the position of the low-level jet. The variation and signs of both components of the momentum flux are consistent with the formation of a low-level jet and in fact are

mandatory in order to achieve a steady balance between the pressure gradient forcing and stress divergence. With swell the balance of terms is opposite to that of a conventional PBL, the stress divergence serves to accelerate the u-component of the wind while the pressure gradient acts to retard the flow. Finally, notice that with small amounts of convection the vertical momentum flux uW is small but clearly positive over the vertical extent $30\text{m} < z < z_i$. We speculate that surface convection transports positive signed vertical momentum, generated by swell, to the upper regions of the PBL.

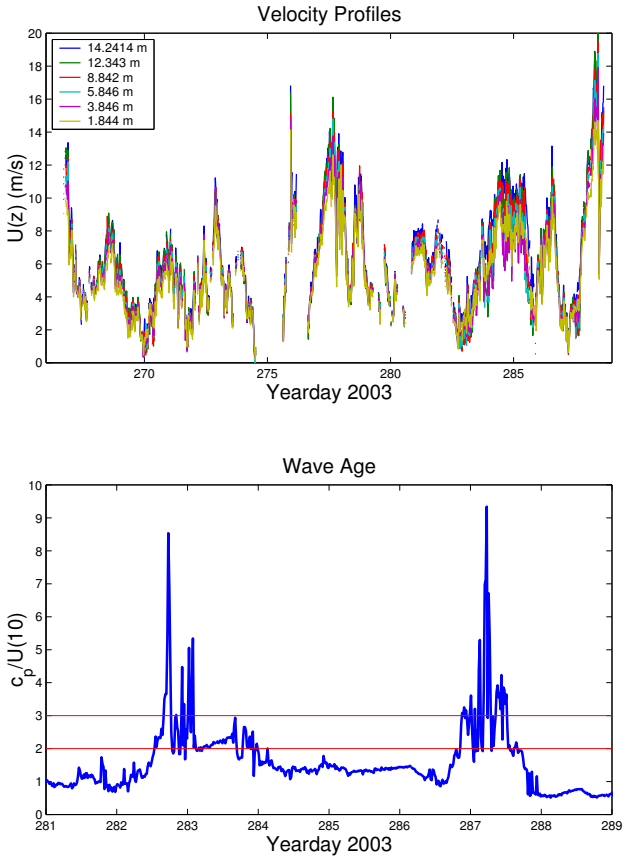

Figure 6: Observations from the CBLAST field campaign. Upper panel mean velocity at 6 levels in the marine surface layer. Lower panel wave age c/U_{10} for a selected time period showing conditions with growing, fully-developed, and swell waves. The horizontal lines indicate data used to compute bin averaged velocity profiles for swell conditions.

4. CBLAST OBSERVATIONS

The goal of the CBLAST low-wind observational program is to improve our understanding of air-sea interaction and provide a database for model comparison and evaluation (see CBLAST (2004) for further details). The intensive CBLAST observation period, approximately two months in duration, occurred in the late summer of 2003 and gathered data using a variety of platforms. One of the novel measuring components is a low-profile air-sea interaction tower which allows detailed turbulence measurements close to the air-water interface. In the atmospheric surface layer, two vertical masts were deployed from the tower: a fixed flux mast designed to gather high resolution turbulence data at six fixed vertical levels and a vertically traversing mast that collected mean profile information over a range of heights above the sea surface. In addition to the turbulence information a detailed set of wave measurements were also collected (Edson et al., 2004).

Here we present a small subset of atmospheric data collected from the profiling mast along with wave information. The two panels of Figure 6 show the variation of the mean wind speed (20 minute averages) at six different levels obtained over the course of the observational period. The data is dominated by low wind conditions, $\langle u \rangle \approx 5\text{ms}^{-1}$, with some persistent conditions where the winds exceed 10ms^{-1}. In the lower panel of Figure 6, wave age c/U_{10} is shown for a subset of eight days. Within this time frame, we observe periods dominated by swell, $c/U_{10} > 2$. Bin averaged velocity profiles based on the wave age brackets $c/U_{10} = [0,1],[1,2],[2,3]$ are shown in Figure 7. The vertical profiles of the mean velocity clearly illustrate a sea state dependence. For the case dominated by swell, a clear departure from Monin-Obukhov predictions are observed as a low-level jet tends to form in the region between $6\text{m} < z < 16\text{m}$. We note that only data obtained under unstable conditions is used to construct these profiles. The observations and LES predictions for unstable conditions are in good qualitatively agreement. The velocity profiles from the observations and LES are nearly uniform over the same vertical extent and both display weak low-level jets in the surface layer. A comprehensive comparison between LES and CBLAST observations is a topic of future research.

5. DISCUSSION AND CONCLUSIONS

There is a striking similarity between the present LES solutions and observations of swell dominated marine boundary layers. The formation of a jet or in some instances a near uniform velocity profile in the vicinity of the waves is consistent with past and current surface layer observations of Holland et al. (1981), Miller (1999) and Edson et al. (2004). These investigations find that the region influenced by swell can exceed the height of the measuring mast, approximately $0 < z < 15\text{m}$. Hence, LES and observations both find that swell invalidates the notion of a shallow WBL. The influence of swell is not

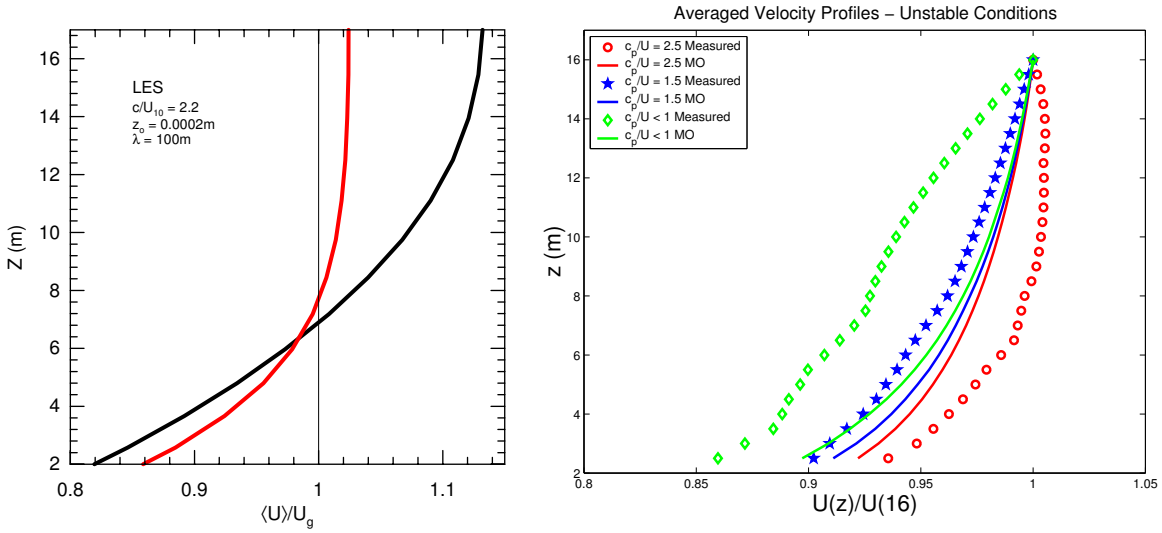

Figure 7: Vertical wind profiles in the marine surface layer computed from LES (left panel) and observed during CBLAST (right panel). The LES profiles for flow over swell, taken from Figure 3, are cases with neutral stratification (black line) and weak unstable stratification (red line). The observations show velocity profiles for cases with growing waves (green symbols), fully-developed waves (blue symbols), and swell waves (red symbols). For each condition, the Monin-Obukhov predictions are shown as solid lines.

confined to the surface layer. Fast moving swell upsets the turbulence production mechanism in the marine surface layer which in turn impacts the whole PBL. In the absence of shear production, turbulence in the upper PBL tends to collapse and the wave-driven PBL differs from its counterpart with stationary surface roughness. Thus the LES supports some of the findings reported by Smedman et al. (1994, 1999). The appearance of a low-level jet and vertically varying vertical momentum flux make surface layer measurements dependent on wave state and vertical distance above the surface thus invalidating the Monin-Obukhov method of predicting surface fluxes in agreement with Rutgersson et al. (2001). The current LES with its monochromatic wave represents an idealization of a light wind following swell. In the open ocean, a multi-component wave field can simultaneously be a sink and source of momentum for the atmosphere, with short (long) waves extracting (imparting) momentum. The sign and magnitude of the near surface fluxes will then depend on several factors including the orientation of winds and waves and the relative location of the wave spectral peak and the mean wind. Flux parameterizations thus require information about the wave field.

Acknowledgments: NCAR is sponsored by the National Science Foundation. PPS and JBE are supported by ONR (CBLAST). We thank Stephen Belcher, Edward Patton, and Anna Rutgersson for their insights during the preparation of this work.

REFERENCES

Belcher, S. E. and J. C. R. Hunt, 1998: Turbulent flow over hills and waves, *Annual Review of Fluid Mechanics*, **30**, 507–538.

CBLAST, 2004: http://www.whoi.edu/science/aope/dept/cblast/low/cblastlow.html.

Cohen, J. E. and S. E. Belcher, 1999: Turbulent shear flow over fast-moving waves, *J. Fluid Mech.*, **386**, 345–371.

Donelan, M. A., W. M. Drennan, and K. B. Katsaros, 1997: The air-sea momentum flux in conditions of wind sea and swell, *J. Phys. Oceanogr.*, **27**, 2087–2099.

Drennan, W. M., K. K. Kahma, and M. A. Donelan, 1999: On momentum flux and velocity spectra over waves, *Boundary-Layer Meteorol.*, **92**, 489–515.

Edson, J. B., R. F. Crofoot, W. R. McGillis, and C. Zappa, 2004: Investigations of flux-profile relationships in the marine atmospheric surface layer during CBLAST, in *16th Amer. Meteorol. Soc. Symp. on Boundary Layers and Turb.*, This Volume, Portland, ME.

Grachev, A. A. and C. W. Fairall, 2001: Upward momentum transfer in the marine boundary layer, *J. Phys. Oceanogr.*, **31**, 1698–1711.

Grachev, A. A., C. W. Fairall, J. E. Hare, J. B. Edson, and S. D. Miller, 2003: Wind stress vector over ocean waves, *J. Phys. Oceanogr.*, **33**, 2408–2429.

Harris, D. L., 1966: The wave-driven wind, *J. Atmos. Sci.*, **23**, 688–693.

Holland, J. Z., W. Chen, J. A. Almazan, and F. C. Elder, 1981: Atmospheric boundary layer, in *IFYGL-The international field year for the Great Lakes*, edited by E. J. Aubert and T. L. Richards, pp. 109–167, NOAA, Ann Arbor, MI.

Makin, V. K. and C. Mastenbroek, 1996: Impact of waves on air-sea exchange of sensible heat and momentum, *Boundary-Layer Meteorol.*, **79**, 279–300.

Miller, S. D., 1999: *The structure of turbulent and wave-induced wind fields over open-ocean waves*, Ph.D. thesis, University of California Irvine.

Moeng, C.-H., 1984: A large-eddy-simulation model for the study of planetary boundary-layer turbulence, *J. Atmos. Sci.*, **41**, 2052–2062.

Rutgersson, A., A. Smedman, and U. Högström, 2001: Use of conventional stability parameters during swell, *J. Geophys. Res.*, **106**, 27117–27134.

Smedman, A., U. Högström, H. Bergström, and A. Rutgersson, 1999: A case study of air-sea interaction during swell conditions, *J. Geophys. Res.*, **104**, 25833–25851.

Smedman, A., M. Tjernström, and U. Högström, 1994: The near-neutral marine atmospheric boundary layer with no surface shearing stress: A case study, *J. Atmos. Sci.*, **51**, 3399–3411.

Sullivan, P. P. and J. C. McWilliams, 2002: Turbulent flow over water waves in the presence of stratification, *Phys. Fluids*, **14**, 1182–1195.

Sullivan, P. P., J. C. McWilliams, and C.-H. Moeng, 1994: A subgrid-scale model for large-eddy simulation of planetary boundary-layer flows, *Boundary-Layer Meteorol.*, **71**, 247–276.

—, 1996: A grid nesting method for large-eddy simulation of planetary boundary layer flows, *Boundary-Layer Meteorol.*, **80**, 167–202.

—, 2000: Simulation of turbulent flow over idealized water waves, *J. Fluid Mech.*, **404**, 47–85.

Thomson, J. F., Z. U. A. Warsi, and C. W. Mastin, 1985: *Numerical Grid Generation: Foundations and Applications*, North-Holland, 483 pp.